# STRENGTHENING MASONRY VAULTS WITH ORGANIC AND INORGANIC COMPOSITES: AN EXPERIMENTAL APPROACH

Leire Garmendia[a,b], Pello Larrinaga[a], Rosa San Mateos[a], José T. San-José[c,*]

[a] *TECNALIA. c/Geldo, Ed. 700, Parque Tecnológico de Bizkaia, 48160, Derio, SPAIN*
[b] *UPV/EHU, Dep. of Mechanical Engineering. c/Rafael Moreno Pitxitxi nº2, 48013 Bilbao, SPAIN*
[c] *UPV/EHU, Dep. Mining, Metallurgical and Mat. Science, Alameda Urquijo s/n, 48013 Bilbao, SPAIN*

## Abstract

Polymer-reinforced fibres are now commonly applied to buildings for structural retrofitting purposes. These materials add greater tensile strength to structures, at the expense of a slight increase in weight. However, they also have other disadvantages such as brittle behaviour and lack of water vapour permeability, which are not desired in the conservation of heritage buildings.

Alternative composite materials embedded in an inorganic matrix are presented, which solve some of the drawbacks associated with organic matrices. Long steel fibres and basalt textiles are applied to the resistant core of the inorganic matrix to produce a steel-basalt reinforced mortar-based composite. Firstly, a mechanical characterization of the individual components and the resulting material was performed. Secondly, non-strengthened and strengthened real-scale (2.98 m span, 1.46 m high and 0.77 m deep) brick masonry vaults were tested up to failure, in order to demonstrate the mechanical effectiveness of these composite materials. Finally, a comparison between two mortar composite materials (steel-strips/basalt-textiles embedded in a polymer matrix) was performed, with the same real-scale brick-vault failure tests.

The experimental campaign demonstrates that the steel/basalt composite mortar is a feasible alternative, which is physically compatible with masonry structures, easy to apply and effective for the reinforcement of brick vaults.

*Keywords:* basalt, mortar, polymeric, steel, strip, textile

## 1. Introduction

Externally Bonded (EB) composite materials are fast becoming the standard solution for structural strengthening, substituting traditional techniques (reinforced concrete, steel, etc.) that can shorten the lifespan of the structure and alter its esthetic appearance. Various research works have demonstrated that EB materials find appropriate solutions and perform well when applied to masonry structures that are at severe risk of deterioration and collapse over time [1-3].

Fibre Reinforced Polymers (FRP) based on unidirectional sheeting embedded in an organic matrix were introduced in the 90s. Over the past two decades, the reinforcement of arches and vaults using FRP materials have provoked great interest and several experimental studies have shown evidence that it is a valid option for strengthening and/or repairing masonry [4-8], particularly, arched masonry structures [9-12]. Setting the most interesting advantages of FRP aside, the results obtained so far may hardly be considered satisfactory in

* Corresponding author. Tel.: +34 946014080.
E-mail address: josetomas.sanjose@ehu.es (José T. San-José).

terms of a lack of ductility, sensitivity to high temperatures, cultural incompatibility (surfaces of ancient and stony substrates), etc.

The present research is focused on inorganic matrix composites, i.e. Textile Reinforced Mortar (TRM) and Steel Reinforced Mortar (SRM) [13-15], which offer advantageous solutions due to their water-vapour permeability, applicable over humid substrate (common situation in masonry structures), lack of toxic substances emission in case of fire, fire resistance, ease-of-application and of removability. Although their mechanical properties in comparison to organic composites can be less effective, and may require longer curing periods (weeks), for example, their overall behaviour makes them an attractive solution for the retrofitting of masonry structures [16-18]. TRM and SRM solutions are designed to preserve existing masonry structures and to prevent brittle failure. For this purpose, constitutive materials of the composite must be appropriately selected.

The effectiveness of EB reinforcement is highly dependent on the bond between the composite and the substrate, and the interaction between the matrix and the inner reinforcement. Interface behaviour and the mortar-reinforcement bond are therefore key factors in the performance of the strengthening technique. Hence, the most important characteristics of the matrix should be as follows: adequate consistency to penetrate the textile (dependent on textile density and geometry), workability, chemical and physical compatibility with the substrate, adequate mechanical properties, low creepage and shrinkage, and good fire resistance.

Bidirectional textiles (TRM) of a different nature (basalt, glass, hemp, etc.) and unidirectional steel fibres (SRM) are both used in the inner reinforcement of the composite. The fibre quantity and the geometrical distribution of the textile, i.e. the spacing of rovings and their direction, can be independently controlled, thereby affecting the mechanical characteristics of the textile and the degree of penetration of the mortar through the mesh openings (cells) [19].

The transmission of effort from matrix to steel cords in SRM is through their adherence between each other. Long steel fibres and basalt textiles are applied to the resistant core of the inorganic matrix to produce a steel-basalt reinforced mortar-based composite. In the case of TRM, bidirectional textiles such us BRM (basalt fibres embedded in the EB matrix) are usually applied, in order to improve bond behaviour. Normally, when loads are applied in a single direction, transversal fibres are designed to maintain roving spacing and to improve the bond between textile and matrix. When the main material is too expensive or difficult to mesh, longitudinal fibres are placed onto an orthogonal mesh composed of an adaptable and cheap compound. Fig. 1 presents both cases that are studied in the present paper: cords/strips (made of steel) and basalt textile.

This research work investigates BRM and SRM retrofitting of masonry vaults, among other solutions, which is novel area of experimental research. Recent studies on the strengthening of arches [20-21] and walls [18] with inorganic-based composites have demonstrated that their structural behaviour improves, in terms of ultimate load and displacement. However, very little work has been done on arched structures strengthened with BRM and SRM and further investigation is essential prior to the development of real applications.

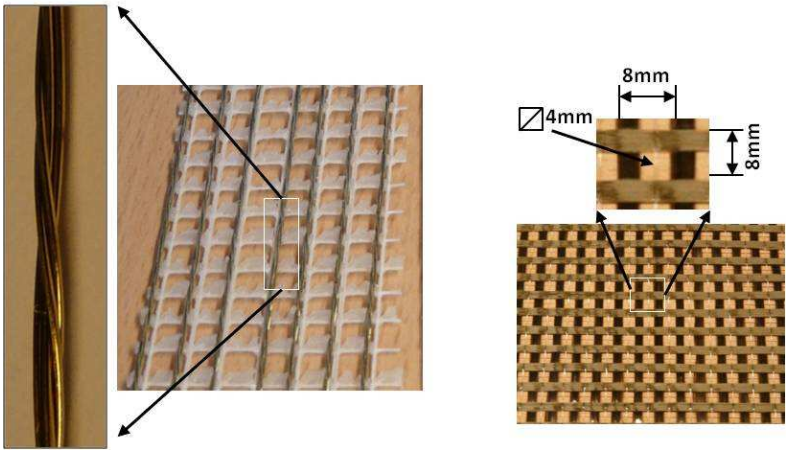

Fig. 1. Steel cords and strips made of steel wire (left) and basalt textile (right).

## 2. Objective

Our aim is to contribute to the conservation of the structural integrity of our historical heritage through an in-depth study of a reinforcement system for brick vaults. This study seeks to contribute to expanding our knowledge on the behaviour of brick masonry vaults and the effectiveness of a reinforcement system based on basalt textiles and steel cords, embedded in inorganic matrices, known as Basalt and Steel Reinforced Mortar: BRM and SRM, respectively.

The first step was to perform a mechanical characterization of the materials. In a second step, the experimental work on masonry arches (constructed with the same materials and geometry as in real structures) was designed, in order to fulfil the following objectives: to characterize the structural behaviour of non-strengthened vaults and to study the influence of the BRM/SRM strengthening system on the behaviour of the vaults as it relates to the failure mode, load bearing capacity and deformation. In a final step, vaults strengthened with Basalt and Steel Reinforced Polymer (BRP and SRP, respectively) were tested to perform a structural evaluation and comparison.

As clearly stated by Dr. Valuzzi et al. [2], EB strengthening composite solutions always increase the ultimate strength of masonry structures, but this increased strength is not always accompanied by higher ductility. Therefore, further research should be conducted to assess whether EB composites can prevent brittle collapse. In line with this objective, the novel aspect of this present paper is mainly based on the combination of three main aspects. Firstly, the constituent materials combined in the studied TRM composites. Secondly, the structural evaluation focused on two completely different EB composites (due to their specific matrices): organic (wet lay-up) vs. inorganic (lime mortar). And, thirdly, the experimental approach applied in the tested vaults: masonry type (erected with materials and geometry presented in real cases), structural test lay-out (asymmetric load configuration) and the vault dimensions (full-scale)

The non-strengthened (one case study) and the strengthened (the other case study) vaults are separately considered due to their different characteristics. These two vault types have been discussed in terms of load (initial linear behavior and load-bearing capacity) versus deformability. Further discussion and related experimental work involving analytical and numerical approaches is an area for future research.

## 3. Material Characterization

This section describes the mechanical characterization of the materials found in the brick masonry specimens (component level) and the reinforcement system (composite level).

### *3.1. Masonry: brick, bedding and matrix mortar*

The vaults were constructed with solid facing "Rosso Vivo - A6R55W" clay bricks (250 x 120 x 55 mm) from San Marco-Terreal (Italy). These soft mud bricks have two different surfaces: one face is rougher and more porous than the other more refined surface. In total, 18 bricks -six per test- were used in the material characterization tests. Compressive strength ($f_{cm}$) tests were based on Standard EN 772-1:2001 [22]. The value of the elastic modulus (E) was calculated in accordance with Standard UNI 6556:1976 [23] while the flexural strength ($f_{tm}$) was performed following the specifications stated in Standard EN 67042:1988 [24]. These mechanical properties are included in Table 1.

Table 1. Average mechanical properties of the materials

| | $f_{cm}$ [MPa] | $f_{tm}$ [MPa] | E [GPa] |
|---|---|---|---|
| Brick | 19.8 (2.5%) | 3.7 (4.3%) | 5.76 (5.2%) |
| Bedding mortar | 7.3 (0.1%) | 1.9 (0.12%) | 6.11 (24.7%) |
| Matrix mortar | 21.3 (7.1%) | 5.8 (16.5%) | 16* |

** According to technical data sheet* *Coefficient of variation in brackets*

The bedding mortar, composed of FEN-X/A, was a natural hydraulic lime (from Arte Constructo bbva company), including a binder and selected aggregates with a maximum grain size up to 4 mm; it is of medium to high strength, with a low content of water-soluble salts. A mineralogical analysis was performed using the powder X-ray diffraction technique, where the diffractometric measurements were taken using a Philips X'Pert Pro MPD pw3040/60 diffractometer equipped with a copper ceramic tube. As can be observed in Table 2, the mortar is mainly dolomite and calcite, commonly referred to as lime mortar.

Table 2. Mineralogical characterization of bedding and matrix mortars

| Mineral Phase | Bedding mortar | Matrix mortar |
|---|---|---|
| Belite [$Ca_2SiO_4$] | • | • |
| Calcite [$CaCO_3$] | ••• | ••• |
| Oxide aluminium and calcium hydrated carbonate [$Ca_8Al_4O_{14}CO_2 \times 24H_2O$] | • | • |
| Quartz [$SiO_2$] | • | • |
| Dolomite [$CaMg(CO_3)_2$] | ••••• | ••••• |
| Ettringite $Ca_6A_{l2}(SO_4)3(OH)_{12} \times 26H_2O$] | • | • |
| Portlandite [$Ca(OH)_2$] | • | • |
| Gypsum [$CaSO_4 \times 2H_2O$] | • | • |

*Black dots indicate the relative abundance of the mineral*

The mortar used to constitute the strengthening composite material (SRM/BRM) was HD System TD13K from Tassullo (Italy) that is manufactured with hydraulic lime mortar to avoid physical-chemical incompatibilities between the substrate masonry and the strengthening material. Following the same procedure as for a bedding mortar, the mineralogical analysis of the matrix mortar established that its chief

constituents were likewise mainly dolomite and calcite. In terms of mechanical expectations, this mortar should have a low enough stiffness to achieve the required ductility of the masonry vaults, in relation to the bonding (plastic hinges formation), unlike the EB matrix mortar, the structural response (stiffer behaviour) of which is needed for its strengthening role in the composite. As may be seen in Fig. 2, the compression and flexural strengths are almost constant as from 28 days of age up until the end of the 180 day test period.

As regards the matrix mortar, some specimens were cast and stored at room temperature and at a controlled relative humidity (20±1 ºC and RH 60±1 %). Three specimens measuring 40 x 40 x 160 mm were tested for flexural strength and, subsequently, six specimens measuring 40 x 40 x 40 mm were tested for compression strength at 28 days, as per standard EN1015-11:2000 [25]. The modulus of elasticity was obtained following Standard ASTM C 469:2002 [26] from three cylindrical specimens with a size of Ø100 x 200 mm. All the results are presented in Table 1. In addition, a total of three specimens were tested for flexural and compressive strength at 7, 14, 28, 60, 90 and 180 days, respectively, to analyze the evolution of their strength in terms of mortar age.

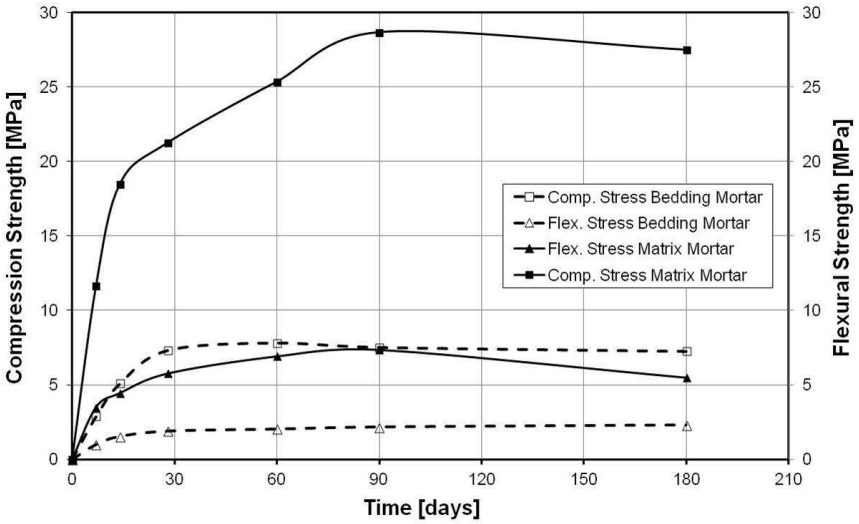


Fig. 2. Strength evolution of bedding and matrix mortars.

Moreover, the variation in strength as a function of mortar matrix age (between 28 and 180 days), which almost maintained a constant flexural strength (Fig. 2), was also determined. It can be seen how the compressive strength increased by almost 35% from 28 to 180 days of age; additionally, the matrix mortar as required possessed a higher stiffness than the bedding mortar under compression and flexural loading, which would be necessary for strengthening purposes.

*3.2. Reinforcement cores of composite: basalt textile and steel strip*

The key properties of the reinforcement cores of the strengthening mortar-based composite are characterized in the present section: steel (cords and strips) and basalt (roving and textile), of the TRM composites (SRM/BRM).

Steel wires (Fig. 1) were used to form cords that are assembled in a polypropylene grid to form what is commercially known as Low Density Steel strips [27]. The unidirectional cords consist of three twisted steel filaments coated in bronze (used in the manufacture of automobile tire reinforcements).

The basalt is spun from selected basalt rocks pre-treated and melted at high temperatures (1400ºC). Basalt fibres are a non-toxic and completely inert material with a low humidity absorption rate and excellent heat resistance; showing good natural adhesion to a broad range of binders, coatings and matrices (lime mortars for example). Basalt fibres, the common mechanical properties of which are given elsewhere [28-29], are mainly constituted by several oxides: $SiO_2$ (54%), $Al_2O_3$ (17%), CaO (6%), $Fe_2O_3$ (7%), among others. Table 3 presents the basic theoretical specifications for the basalt rovings and the steel cords provided by the manufacturers, from the point of view of a specific application, while the specific test results are shown in Table 4.

Table 3. Mechanical characteristics of steel cords and basalt rovings

| Property | Basalt roving | Steel cords |
|---|---|---|
| Ultimate tensile strength [MPa] | 3080 | 3200 |
| Tensile elastic modulus [GPa] | 95 | 206 |
| Ultimate tensile strain [%] | 3.15 | 1.6 |
| Design thickness [mm] | 0.053 | 0.075 |
| Design Area [$mm^2$] | 0.053×8 | 0.481 |
| Weight of the dry sheet [$g/m^2$] | 200 | 600 |
| Density [$g/cm^3$] | 2.8 | 8 |

The steel (cords and strips) and basalt (rovings and textile) strengthening solutions were mechanically characterized in the laboratory by means of uniaxial tensile tests (seven samples in each test). Tests were performed on 100 mm wide and 600 mm broad-specimens of single steel cords and basalt rovings (Fig. 3).

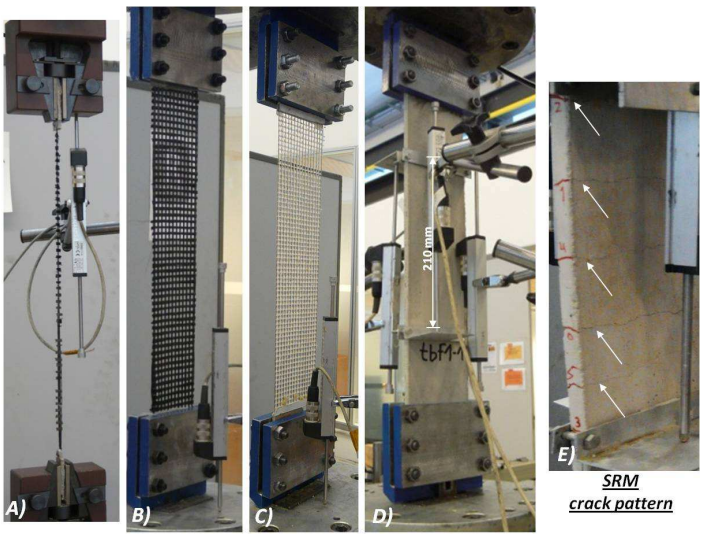


Fig. 3. Tensile test lay out: A) basalt roving; B) basalt textile; C) steel strip; D) SRM/BRM; E) detail.

The test results, which refer to sixteen steel cords and twelve basalt rovings, are summarized in Table 4 and displayed in Fig. 4. Tests were performed on a Schenk 100kN universal testing machine model, with automatic displacement control and a load measurement precision of over 0.3% for reading up to 1kN. Seven specimens of one steel cord and seven steel strips were tested in accordance with internal procedure, which was based on Standard ASTM D5034-95(2001) [30] and two previous tests reported in the literature [13, 31]. The testing machine displacement rate was 1 mm/min, according to results obtained by Dr. García [32]. All the information was compiled with an MGC-Plus Data Logger at a frequency of 5Hz.

Table 4. Main mechanical results under elastic behaviour in reinforcement tensile tests

| Material | $f_r$ [N] | $\sigma_r$ [MPa] | $\varepsilon_r$ [%] | $E_r$ [GPa] [5] |
|---|---|---|---|---|
| Steel cord | 1219 (2%) | 2535 (2%)[1] | 1.90 (8%) | 133 (8%) |
| Steel strip | 23734 (8%) | 3165 (8%)[2] | 2.20 (12%) | 144 (8%) |
| Basalt roving | 240 (19%) | 565 (19%)[3] | 0.80 (21%) | 71 (5%) |
| Basalt textile | 2680 (22%) | 505 (22%)[4] | 0.80 (21%) | 63 (4%) |

[1] $\sigma_r = f_r / (0.481)$; [2] $\sigma_r = f_r/(0.075\times100)$; [3] $\sigma_r = f_r / (0{,}053\times8)$; [4] $\sigma_r = f_r / (0{,}053\times100)$; [5] $\sigma_r/\varepsilon_r$

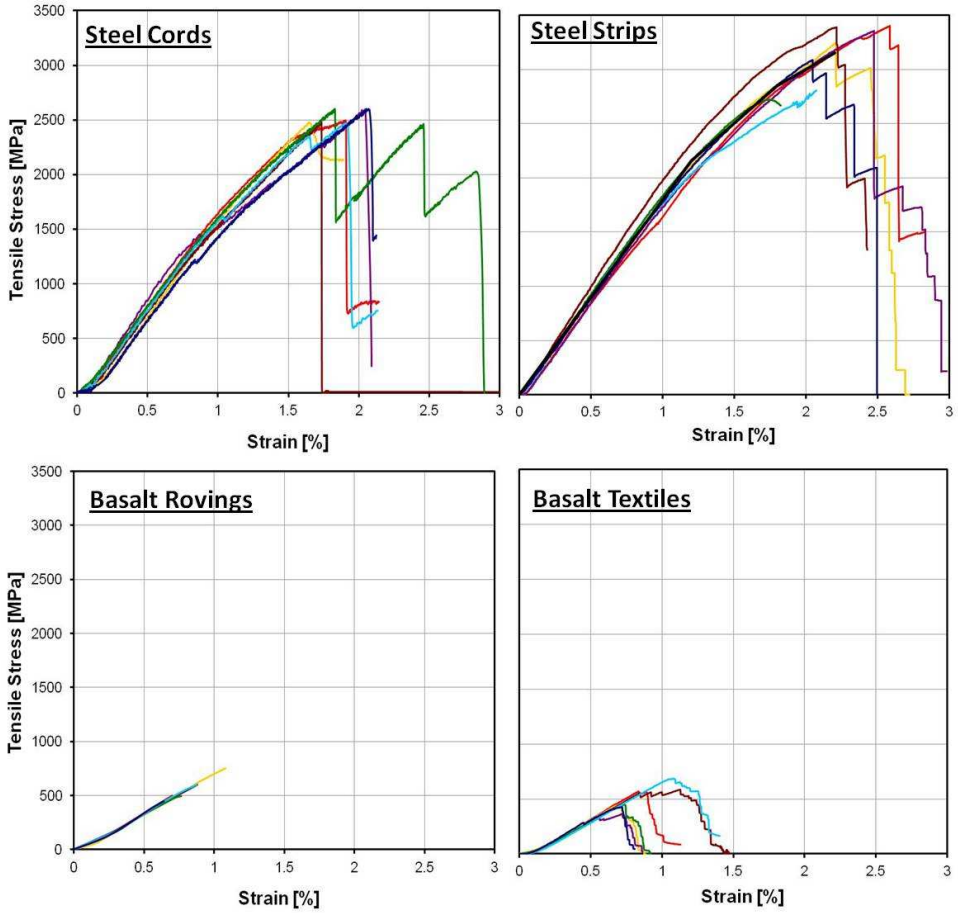


Fig. 4. Tensile test of steel cords/strips and basalt roving/textile.

Failure was caused by stress concentration in the clamps, as is usual in high strength-low ductility steels, due to the high strength value of steel strip. It explains why the ultimate load value of the material was never reached. Hence, the results were only valid for the secant elasticity modulus ($E_r$) of the material, calculated

as the rate between the average value of the maximum tension stress ($\sigma_r$) and its respective strain ($\varepsilon_r$). The high scattering of the basalt stress-strain values (above 20%), as opposed to the steel stress-strain values (on average 10%) should be underlined.

The absence of any coating on basalt roving/textile, which would have enhanced the effectiveness of all the fibres included in each roving [13], and the non-uniform load distribution in the textile width, explain these lower values (over 20%) in comparison to the supplier specifications in Table 3, apart from the large scatter registered (at ultimate loads, but not under elastic behaviour, as shown in Fig. 4), especially in the textile specimens (the large number of rovings increased this problem).

The high loads recorded in the steel-strip tests (>23kN) were a precaution against any possible loss of adherence force between the steel cords and the mortar. On the contrary, the basalt textiles developed a tensile strength that was on average 10% lower than the basalt roving and 6 times lower than the steel strips.

### *3.3. Mortar based composite*

With the purpose of analyzing the tensile behaviour of the global mortar composite SRM/BRM, seven single-ply steel strips and seven single-ply basalt-textile specimens, of 600 mm in length, with a cross-sectional area of 100 mm x 10 mm, were cast. The established test set-up and geometry of the specimens were based on previously published works [33-34] including two by the authors [13, 27]. The samples were prepared in plywood formworks and, after casting, the fourteen specimens were held in a saturated atmosphere for seven days, and were then stored for 21 days in a controlled environment (18±1 ºC and RH 60±1 %). All the specimens were tested between 28 and 34 days of age.

The internal layer (800 x 100 mm) was positioned in the middle of the cross section. Since high loads were expected in this test, special considerations were taken in the design of the specimens and in the fastening system for the test (Fig. 3, sketches D and E). The SRM/BRM specimen geometry was not very long and the anchorage length might have been insufficient to avoid slippage. Therefore, extra strips/textile at both ends (length 100 mm) of the internal reinforcement were folded over (180º) and immersed in the fresh mortar. Due to this action, the failure of the specimen was promoted in its central position (210 mm, as indicated in Fig. 3D).

The SRM/BRM tensile specimens were placed in the same Schenk 100kN testing machine with a controlled load under a deformation rate of 0.5 mm/min. The deformation of the central position (210 mm length) was measured by means of four Novotechnik TRS 100 displacement transducers (Fig. 3), obtaining several stress-strain curves under the uniaxial tensile test, as presented in Fig. 5.

The tensile behaviour of the inorganic matrix composites differed from that of the polymeric matrices (FRP), due to the brittleness of the inorganic matrix; the ultimate tensile strain of these materials being considerably smaller than that of the fibres. The organic composites therefore presented an elastic behaviour up to the point of failure, as long as the elastic behaviour of the fibres continued up to failure. Nevertheless, the inorganic matrices cracked before the maximum strain of the strip was reached. The effectiveness of the reinforcement was therefore evident when the matrix started to develop cracks. After cracking, the tensile stress within the cracked cross-section was carried entirely by the filaments (Fig. 3).

As previously observed by Dr. Larrinaga et al. [13, 27] and others [14-15], under pure tension loads, the TRM non-linear stress-strain curves could be divided into three stages, which follow the “cracking model”:

stage I ($\sigma_I$ , $\varepsilon_I$ and $E_I$) ended at the point when the first crack appeared (pre-cracking stage); stage II ($\sigma_I \approx \sigma_{II}$ ,$\varepsilon_{II}$) ended when no further cracks were observed (multiple cracking stage); and, finally, stage III ($\sigma_{III}$ ,$\varepsilon_{III}$ and $E_{III}$ measured as the slope of that stage), when the crack patterns stabilized and the tensile loads increased (post-cracking stage). Therefore, as shown in Figures 4 and 5, there was a degree of load transfer from the matrix to the steel strip and the basalt textile, when the first cracks appeared in the specimens, which are represented by short drops in the loading values of the stress-strain graphs. A summary of the main results from Figure 5 are presented in Table 5.

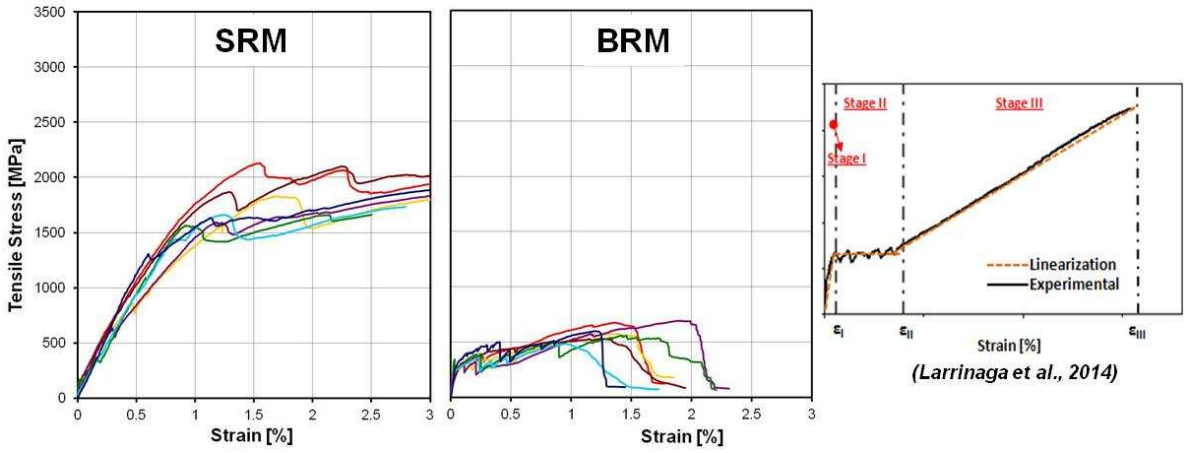


Fig. 5. Stress-strain behaviour in uniaxial tensile test of.

Textile slippage within the matrix was considered. The failure mode of the SRM specimens was caused by cracking and debonding of the composite. At a certain strain level (around 1.2%), the deformation of the composite has a negative effect on the cohesion of the mortar, which could no longer be deformed, hence the rupture of the matrix and the internal slippage of the steel reinforcement. The ultimate load of the strip (3165 MPa, according to Table 4) was therefore never reached (being the maximum value about 50%). The areas for strengthening the vault and arch in the retrofitting process were usually quite large and the in-service strain is low, therefore, the cracking observed in the uniaxial tensile test was not likely to develop, as is confirmed in the following section (tested vaults).

Table 5. Main mechanical results under elastic behaviour in TRM tensile tests

| Material | $f_{III}$ [N] | $\sigma_{III}$ [MPa] | $\sigma_I$ [MPa] | $\varepsilon_I$ [%] | $\varepsilon_{II}$ [%] | $\varepsilon_{III}$ [%] | $E_I$ [GPa] [3] | $E_{III}$ [GPa] |
|---|---|---|---|---|---|---|---|---|
| SRM | 12853(14%) | - | 1714(14%)[1] | 1.20(23%) | - | - | 142(15%) | - |
| BRM | 3173(13%) | 598(13%)[2] | 442(39%) | 0.04(30%) | 0.60(35%) | 1.40(22%) | 1105(17%) | 26.7(4%) |

[1] $\sigma_r = f_r / (0.075 \times 100)$; [2] $\sigma_r = f_r / (0{,}053 \times 100)$; [3] $E_I = \sigma_I / \varepsilon_I$

Unlike SRM, the BRM failure mode was quite different in terms of strength (lower values), ductility (stages I, II and III and less ultimate strain were clearly identified) and stiffness (higher at the pre-cracking stage). With regard to the BRM-based composites, the curves show considerable scatter (values up to 39%). This effect could be caused by the lack of internal reinforcement (only one textile layer), contrary to the application of several textile layers [35]. Despite the scatter, the slope at stage III ($E_{III}$) remained similar in most of the specimens as it is showed in Fig. 5.

When compared with internal reinforcement, the pre-cracking stage performance of SRM was the same in terms of stiffness ($E_r = E_I$), but was 46% lower in terms of strength ($\sigma_r >> \sigma_I$) and had a higher scatter. Unlike the BRM, stages II and III were not clearly recorded (omitted in Table 5). A remarkable observation is the practical absence of stage II in some of the specimens. The Young's moduli varied as the strain increased, stage III was non-linear and therefore $E_{III}$ was not observed. The crack pattern developed during the first steps of the third stage, as observed by Dr. Larrinaga [35]. Hence, load absorption by the SRM composite started earlier than in the BRM series, an interesting feature for a material expected to work as a strengthening solution.

BRM tensile strength was quite similar from the standpoint of the textile and the composite, the ultimate measured deformation was quite low in comparison with SRM (Fig. 5). The BRM early moduli at the post-cracking stage ($E_{III}$) were over 40 times less stiff than its pre-cracking one ($E_I$). These results suggest that the optimistic specifications of the basalt textile manufacturers (Table 3) are not realistic (Table 4), which is a key point for several reasons. Firstly, BRM is composed of denser basalt rovings which implies that the whole fibre surface will not be completely wetted by the matrix (mortar paste). Secondly, the behaviour of a composite in a brittle matrix (mortar) implies that the fibres are held in the matrix solely by the presence of friction. Thirdly, as a result, when the matrix has completely cracked (stage III), only a part of the whole basalt fibres are stressed working.

A key contribution of the uniaxial tensile tests is the possibility of obtaining the Young's Moduli of the composites, which identifies the starting point for load absorption such as a masonry strengthening system, in SRM mortar based composite (pre-cracking stage) and at the post-cracking stage III (habitual working conditions in their masonry strengthening behaviour).

## 4. Masonry vaults

### *4.1. Vault construction*

A total of six barrel vaults (generated from a segmental arch) were built, using clay bricks and lime mortar or bedding mortar (described in section 3.1) the characteristics of which are similar to those observed in mortars commonly found in heritage structures. A 10 mm-thick layer of lime mortar was used in the joints. The geometry and dimensions of the vaults shown in Fig. 6 included the load application line point at a quarter of the span (width or deep vault equal to 0.770 mm).

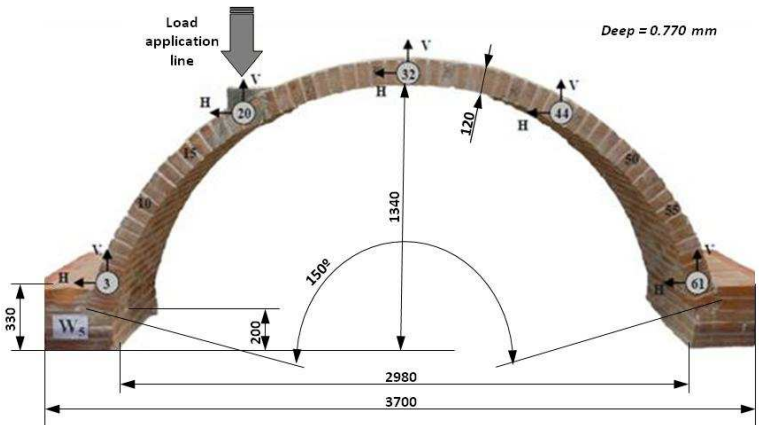


Fig. 6. Test lay-out and dimensions of the vaults.

Two vaults remained non-strengthened (R1 and R2) while the others were strengthened, on the extrados, with externally bonded (EB) solutions: BRM, BRP, SRM and SRP. The objective of this experimental campaign was as follows: (i) to characterize barrel vault behaviour and to contribute to wider knowledge of strengthened and non-strengthened arched masonry structures; (ii) to analyze the effect of EB reinforced mortar as a feasible strengthening solution; and, (iii) to undertake a comparison between the strengthening options, separately assessed and compared with the non-strengthened ones.

The vaults were constructed in an environment with a controlled temperature and at a set relative humidity: RH [44 to 58]±1 % and [17 to 22.5]±1ºC.

The SRM and SRP strengthening solution (Fig. 7) consisted of two 120 mm wide with a measured final strengthening thickness of 15 and 3 mm, respectively, with one ply of embedded steel strip. In the case of SRM, a first 120 mm-wide layer of mortar was applied covering the whole length of the vault, after which the steel strip was positioned in the mortar and, finally, covered with the final mortar layer. Good impregnation of the fibres was ensured throughout the whole process. Concerning the SRP, in the first place, three consecutive ~~a~~ primer layers of SRP were applied, in order to improve the adherence of the organic (resin) matrix and the brick substrate. Afterwards, the application of the matrix took place, the steel strips were placed upon it and, once again, covered with the second resin matrix.

Four spike-anchors were wrapped around the end of each strip in both cases, SRM and SRP (Fig. 7) to prevent debonding at the abutments. These anchors consisted of steel cords inserted into a pre-drilled hole in the brick that was filled with a bi-component epoxy-acrylate styrene-free resin (MOEPSE-W from Index®) acting as a chemical anchor. Half of the length of the spike-anchors was introduced into the brick; the other half was spread outside the brick over the strips.

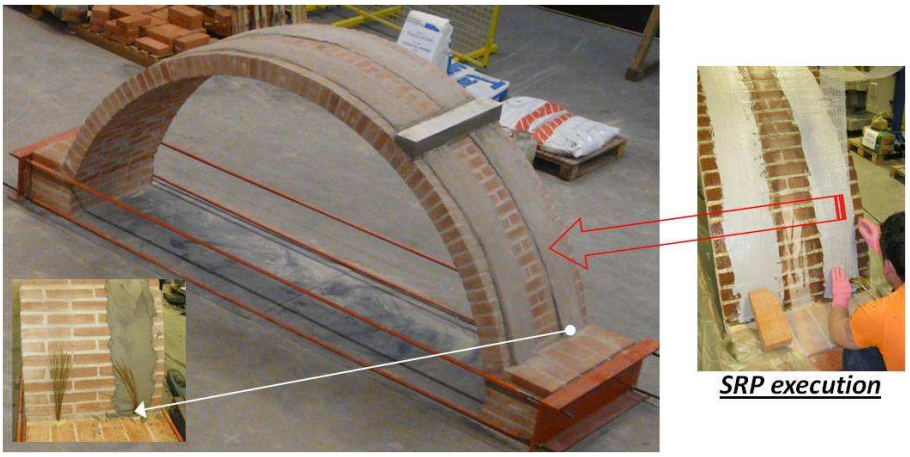


Fig. 7. SRM (left) and SRP strengthened vaults details.

The BRM and BRP (Fig. 8) were applied to the other two vaults in a similar way. In both solutions, a 770 mm-wide basalt ply eventually covered the whole surface of the barrel vaults with the strengthening system that was around 15 and 3 mm thick, respectively.

The BRM lay-out firstly had a base mortar layer, to improve adhesion and to protect the substrate, on which the matrix mortar was applied. Afterwards, a 770 mm wide basalt ply was applied to cover the whole surface

of the vault. Subsequently, a second layer of mortar was applied, ensuring that the textile was perfectly embedded and covered. Additionally (as in SRM), the remaining four spike-anchors were also impregnated with the mortar matrix so that they wrapped the basalt ply at the springers.

Once the eight spike anchors had been placed in position, application of the BRP strengthening system began by applying three consecutive primer layers. When the primers had dried, a first layer of the resin matrix was applied in a very fluid stage, in order to permit the correct soaking of the basalt fibres (subsequently applied to the 770 mm wide basalt ply covering the whole surface of the vault). Finally, a second resin matrix layer was coated, ensuring that the basalt textile was perfectly embedded in the resin matrix. The remaining four spike-anchors were also impregnated with the epoxy resin (wrapped around the basalt ply at both springers).

An arched masonry structure is stable under a given load condition provided that the thrust line, which represents the internal forces at every cross-section, is kept inside the central core (central third of the thickness). When the thrust line moves outside the central core, the formation and consequent opening of a crack takes place and a plastic hinge is formed. The appearance of successive hinges forms a mechanism that triggers the collapse of the structure [36]. The failure of the arch occurs when four hinges are formed.


Fig. 8. Details of BRP and BRM strengthened vaults.

The strengthening system serves to absorb the tensile stress that the arch would not have otherwise withstood. Thus, the thrust line can lie away from the thickness of the arch, increasing its deformability capacity, and delaying its collapse. In the case of reinforced vaults, four failure mechanisms should therefore be considered: masonry crushing, sliding at the hinges, debonding of the reinforcement due to forces perpendicular to the surface and reinforcement breakage [20-21, 37-39].

*4.2. Vault testing lay out*

The tests were performed at the same location where the vaults had previously been constructed, by means of a load application jack suspended from an adjustable metallic framework (Fig. 9). Abutment displacement was constrained by two metallic profiles located at both abutments and tied with four rods.

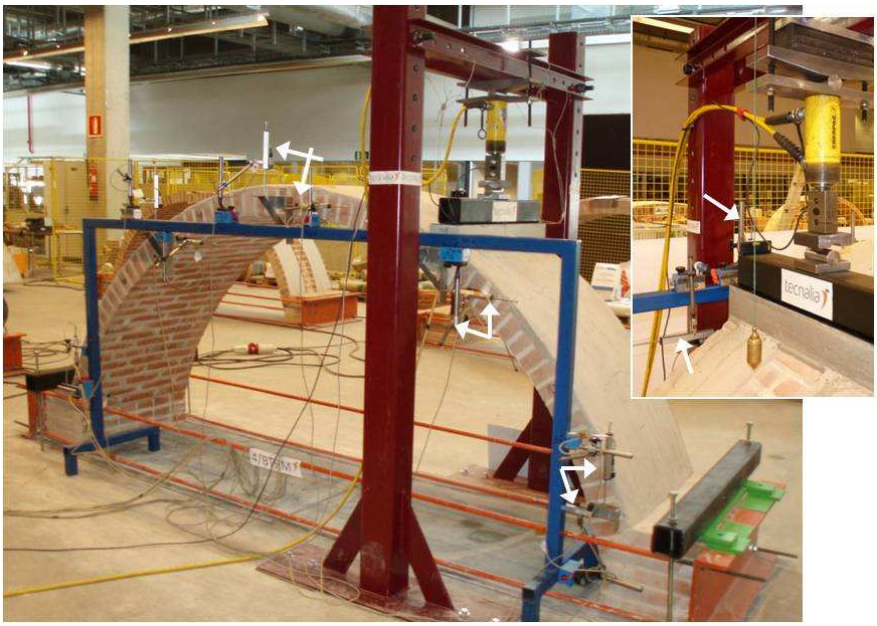

Fig. 9. Vault test set up.

The vertical and horizontal displacement (caused by the appearances of plastic hinges and fissures in the reinforcement) slightly affects the original test geometry. For this reason the load was applied on a sufficiently wide base (large) and through the action of a platen, continuously controlling its vertical descent (Fig. 9). The load was positioned at one quarter of the span and was applied over the whole upper surface of the affected voussoirs (linearly applied on the whole vault width) to provoke failure. The test continued up until failure, using displacement control. The testing speed began at 0.3 mm/min and, afterwards, when the registered displacement reached 10 mm, was increased to 0.6 mm/min. The applied load was measured using a 50 kN capacity S9M force transducer from HBM.

As shown in Fig. 9, during the tests, both the horizontal and vertical displacements of the 5 voussoirs (#3, #20, #32, #44 and #61, as indicated in Fig. 6) were recorded using Linear LVDTs sensors. Data acquisition (software MGCplus from HBM) of the information was recorded at a frequency of 10 Hz, in order to obtain an accurate picture of the failure moment. Besides, continuous visual inspections were carried out during the tests, for the control and recording of hairline cracks, the formation of hinges, failure modes, etc. The experimental results are summarized in Table 6 and outlined in Fig. 10.

Table 6. Summary of the experimental tests results of applied load vs. vertical displacement in voussoir #20

| Vault | Voussoirs Nr. | | | | Linear Load | | Maximum Load Measured | | Failure Mode |
|---|---|---|---|---|---|---|---|---|---|
| | 1st Hinge | 2nd Hinge | 3rd Hinge | 4th Hinge | Load [kN] | Vertical Displacement in line load [mm] | Load [kN] | Vertical Displacement in line load [mm] | |
| R1 | 22-23 | 35-36 | 6-7 | 61-62 | 3.0 | 0.28 | 4.5 | 0.9 | Mechanism |
| R2 | 26-27 | 45-46 | 59-60 | 6-7 | 4.3 | 0.30 | - | - | Mechanism |
| SRM | 19-20 | 61-62 | 40-41 | 2-3 | 5.8 | 0.24 | 20.4 | 50.0 | Mechanism |
| SRP | 21-22 | 1-2 | --- | --- | 5.7 | 0.40 | 22.1 | 42.8 | Joint sliding |
| BRM | 19-20 | 39-40 | 61-62 | 2-3 | 10.4 | 0.20 | 22.1 | 2.3 | Mechanism |
| BRP | 21-22 | 61-62 | 2-3 | 43-44 | 6.35 | 0.46 | 27.0 | 39.7 | Mechanism |

The displacements summarised in Table 6 are the vertical ones, as measured on voussoir #20 (Fig. 6), on which the vertical testing load was applied, following similar procedures described in previous works by the authors [16-17].

*4.3. Vaults testing results*

In the non-strengthened vaults, from the first peak load (linear load stage), every vault is a different structure due to its particular sliding process, hinge formation history, etc., which means that a structural comparison between the vaults is not strictly possible. Nevertheless, the present investigation is mainly focused on examining the structural improvements, in terms of load-bearing capacity and ductility, due to the application of different externally bonded strengthening solutions. R1 vault collapsed due to the formation of four hinges that turned the structure into a mechanism (Fig. 10), observing load swings as a result of the settlements of the voussoirs, due to irregular crushing of the bonding mortar. The sequences of the appearance and the location of the hinges are presented in Table 6.

It should be noted that the back side of vault R1 had a slightly delayed deflection compared to its front side, in the back where a smaller number of cracks appeared than the front; this non-uniform behaviour (already noted in other tested vaults) justifies the view that these barrel vaults not may be considered simple arches. This fact could be due to: 1) a crack between voussoir 34-35 already existed before the test; and, 2) an initial slight deflection in the right haunch. Vault R1 also failed with no large deformations (when compared with strengthened ones), recording a total displacement (square root of horizontal and vertical square displacements) of 6.0 mm at the collapsing load point. Its final collapse configuration is presented in Fig. 10 and the almost simultaneous appearance of all hinges should be noted in R2.


Fig. 10. Collapse configuration of vaults.

Because of multiple failures during the testing progress (load misalignments and interruptions in data collection from some of the LVDTs), the results for R2 could only be considered up until its linear load stage in Table 6 (omitted in Fig. 11).

With regard to the SRM strengthened vault, an initial trial was performed to check the test configuration, because of the higher loads that the SRM strengthened vaults were expected to withstand in comparison with the R1 and R2 vaults. This initial test finished when the first hinge (Voussoirs #19-#20) appeared and a second hinge was expected at the right haunch of the vault, where a lot of cracking became visible.

Once the test set up was verified, the loading of the vault resumed until its final failure (Fig. 10). The first trial yielded valid results that determined the first peak load and the characteristics of the linear behaviour response of the vault (Table 6): 5.8 kN vs. 0.24 mm under linear loads and 20.4 kN vs. 50.0 mm under maximum loads.

In the case of SRP-vault, the load at the first peak was 5.7 kN while the maximum load was close to 22kN; at the same time a linear and total displacement of the load application point was recorded of 0.40 and 42.8 mm, respectively. As may be noted, in comparison with SRM, the SRP solution resisted hinge formation, although all mortar joints were cracked. Failure was due to sliding at the load application point which provoked the rupture of fibres. It is worth underlining that both vaults showed similar behaviour under linear loading stages and not so very different from non-reinforced vaults.

In the BRM strengthened vault, the first plastic hinge appeared in voussoirs #19-#20 (testing load area). It is worth mentioning that the basalt textile fibres were broken in the area of the second plastic hinge (Table 6), which justifies the very low deformation of the BRM vault, owing to premature textile failure (this aspect was verified by testing an additional BRM vault, resulting, as before, in a similar low ultimate displacement at loading point). Despite its higher stiffness under linear loads (10.4 kN vs. 0.20 mm vertical displacement), this vault formed 4 hinges and its failure mode was also a mechanism (Fig.10). Furthermore, detachment on the left abutment appeared. It seems that the confluence of both brittle elements (matrix mortar and basalt reinforcement) leads to a brittle tensile failure of the TRM in the second hinge and a general failure of the vault with low deformations, as in R1. However, the level of the maximum collapse load is excellent (22.1 kN) and the stiffness of the global structure (slope in the linear initial loading Fig. 11 detail) is the highest of all the tests.

The main results of the BRP strengthened vault are likewise shown in Table 6. Note that some bricks (voussoirs) fell out: #22 at the intrados, #21 and some others in the #40 to #43 voussoirs, which correspond with the first and fourth hinges areas. Besides, the detachment of the BRP strengthening composite and the first, the third and the fourth bricks in the voussoirs close to the hinges should be noted.

Finally, it is interesting to underline how all the tested vaults had a similar deformation value (an average of 0.31 mm) under a linear loading stage, which means that the vaults had similar ductile responses after the strengthening composites started working.

### *4.4. Discussion*

The effectiveness of the retrofitting solutions described in the preceding sections, mainly in terms of additional load-bearing capacity and improved ductility, was analyzed in the experimental campaign. Fig. 11 presents the structural behaviour of the vaults, by means of the load vs. vertical displacement law at the load

application point (voussoir #20). The SRM curve corresponds to its second loading cycle, so it is comparable with the other tested vaults, and it also shows the ultimate bearing capacity.

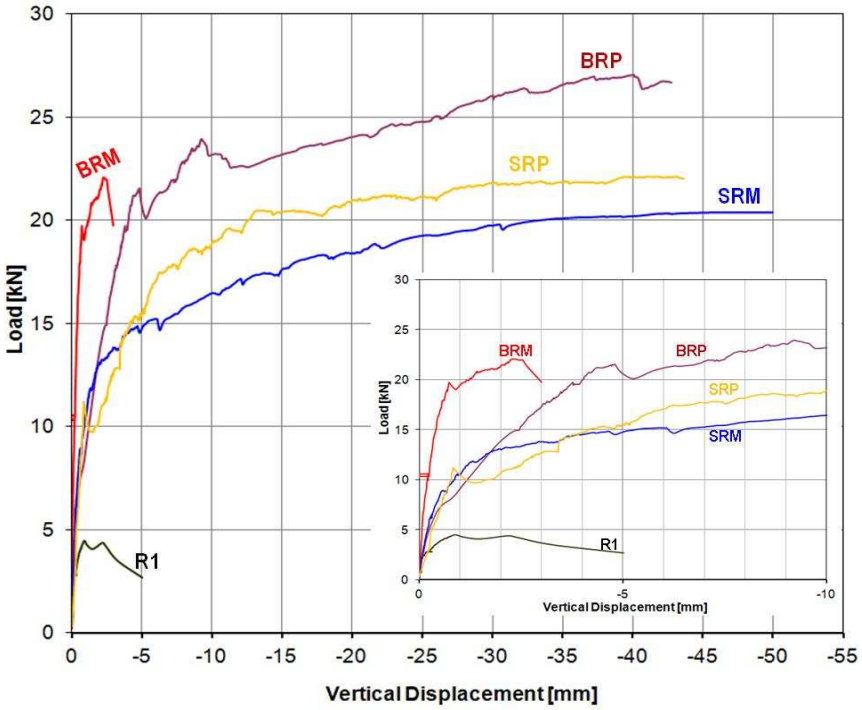


Fig. 11. Load vs. vertical displacements at load application point.

Additionally, some of the horizontal and vertical displacements (voussoirs #3, #20, #32, #44 and #61) in three of the tested vaults are presented in Fig. 12 and the data are reported until the collapse of R1, to gain a better understanding and for an effective comparison between the reinforced and the non-reinforced vaults.

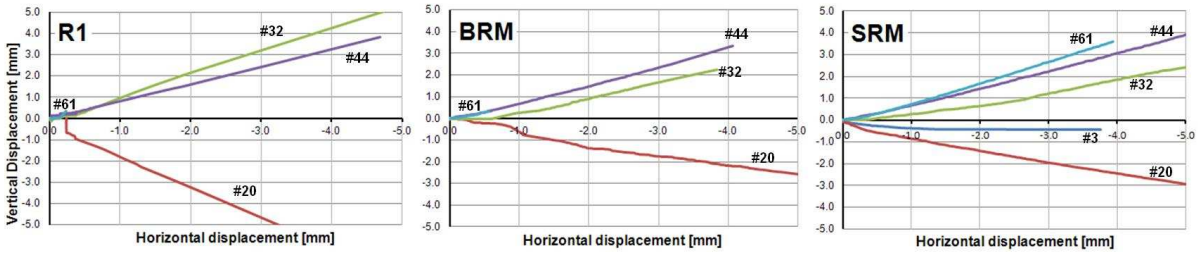


Fig. 12. Horizontal vs. vertical displacements at recorded voussoirs.

From the content of Table 6 and Fig. 11, it may be said that every vault is a different structure, because of its particular failure mode (mechanism or joint sliding), hinge history, EB solution applied, etc. The two non-strengthened vaults (considered as a single group) should therefore be compared with the four strengthened vaults, (also a unique group), and only the linear response, load-bearing capacity and final deformability of both groups of vaults may be discussed.

Any comparison between the SRM/SRP and the BRM/BRP groups of vaults would not yield reliable results due to their different strengthening configuration, in terms of composite geometry (strip vs. textile), material properties (basalt vs. steel) and strengthening core load capacity (different cross sections). So a comparison may only be made between SRM vs. SRP and BRM vs. BRP.

In general terms, all the vaults (strengthened and non-strengthened) reproduced the first hinge (always under the area of load application) and second hinge patterns, at the same branch; with the exception of the second hinge in the SRP vault (see Table 6), the failure mode of which was completely unlike the other vaults under analysis. The differences observed on the third and the fourth hinges could have been caused by inherent heterogeneities in the quality of the masonry or by slight geometric variations in the construction and its order of appearance probably is random.

In the linear load-displacement law, the SRM/SRP and BRM/BRP externally bonded vaults resisted over 50% and 300%, respectively (averaging higher loads) than the non-strengthened vaults. On the contrary, with reference to the maximum achieved linear displacement (loading point), the behaviour of both the strengthened and the non-strengthened vaults was quite similar, except in the BRP vault with the highest linear compliance (lower slope). Pre-cracking (stage I under pure tension loads) of the EB composite mortars caused a similar ductile behaviour in the vaults.

It is worth noting that the ultimate loads capacity of the non-strengthened vaults strongly improved by over 5 times, in terms of their load-bearing capacity, once they had been strengthened by any one of the four solutions. The final (overall) deformability (omitted in Fig. 11) of the strengthened vaults at the collapse stage presented a ductility that was over 40 times higher than the non-strengthened ones. This was not the case of the BRM vault. The BRP vault had a better structural response than the BRM vault, in terms of achieving a higher load-bearing capacity and overall ductility.

The above improvements in the strengthened vaults (failure stage at the highest loads and displacements) implies that the strengthening system absorbed the tensile stresses that the vault would otherwise not have withstood, thus avoiding or postponing the formation of the kinematic mechanism. The trust line can lie outside the thickness of the arch, thus increasing its load resistant capacity and deformability.

The SRM/BRM/BRP strengthening solutions postponed hinge formation while the SRP solution prevented its formation, which meant that the eventual failure mechanism was due to sliding between voussoirs [40], near the keystone. The SRM/BRM strengthening mortar systems allowed us to predict the point at which the future hinges would form, evidence of which were thin cracks that appeared on the mortar surface (a stiffer matrix than the polymeric one). Besides, in a further comparison between the SRM and the SRP vaults, both presented a slightly better structural behaviour, in terms of regularity in the experimental laws of load and displacement, than the BRM/BRP vaults, which developed higher shifts in their load vs. deformation line than the formers.

With regard to the strengthening lay-out, it should be underlined that debonding of the strengthening strips ends could have occurred as they were not extended along the abutments. However, no detachment of the strengthened vaults was observed in the area near the abutments during the testing. This fact implies that the bonded area and spike-anchors at the abutments were sufficient to guarantee adherence between both the strengthening and the substrate. A shear test between the brick work and the composite material would

provide more information on the bond behaviour, which has previously been studied in [41-43], although it lies outside the scope of the present research.

Future research is needed to increase practitioner confidence and to reduce the safety factors associated with these strengthening technologies. However, it could be stated that, the load-bearing capacity increase was significant in all the strengthening patterns, demonstrating that the EB solutions are highly effective at strengthening brick masonry vaults subjected to non-symmetrical vertical loads.

To perform a numerical analysis of the tested vaults is beyond the scope of this paper, although additional comments and initial results are included, based on this study and previous works [44]. The majority of research has focused on novel masonry strengthening solutions based on the FRP formulae [10, 45, 46] which, nowadays, continues to be necessary (for example) to investigate their adaptation to masonry vaults in greater depth.

The previous experience of the authors is based on the use of the FE model and the DBS_ROOF tool [47], as the rigid-block methods applied by the graphic statics and the software programmes are unable to model reinforcements. In view of previous results for the extrados strengthening modelling, the FE model reproduces the behaviour of arched structures in an acceptable manner, but especially in the early loading stages (linear loading behaviour). However, in view of higher loads, and because of the high displacements achieved in masonry structures, is quite complex to obtain a feasible agreement between experimental and analytical results (load vs. displacement laws). For example, the type of contact defined by commercial FE software is unable to guarantee adhesion (above a certain load value) between the vault substrate and the EB strengthening solution.

Table 7 includes some results from the application of specific non-commercial software for vaults and arches, so as to approximate the present research towards an initial analytical baseline. The analytical approach was conducted using Ring 3.0 – LimitState which is based on the rigid block analysis method, the most widely used method for masonry arches and vaults that evaluates the ultimate load of the structure using the principle of virtual works, which assumes that the material behaves in a perfectly plastic and rigid way. As all masonry includes internal discontinuities (mortar joints), the rigid blocks method is a good approach that enables the location of the structural deformation to be simulated. After specifying the geometry and materials of vaults, Ring 3.1 returns the load factor, which gives rise to a thrust line tangent to the thickness of the vault at four points (the thrust line).

Table 7. Comparative results between experimental vs. analytical approaches

| Vault | Maximum Load Measured [kN] | | Failure Mode |
|---|---|---|---|
| | Tested | Ring 3.0 software | |
| R1 | 4.5 | 1.19 | Well predicted |
| SRM | 20.4 | 24.2 | Well predicted |
| BRM | 22.1 | 22.4 | Well predicted |

The results show good agreement in the collapse pattern of three analysed vaults and in the load bearing capacity of those strengthened with TRM composites. However, Table 7 shows a high difference (over 400%) in its load bearing capacity in reference to non-reinforced barrel vaults.

## 1. Conclusions

It is well known that masonry structures present extremely complex bonds between their materials. For example, the volume ratio of mortar/brick strongly affects their structural deformability [48]. Further experimental research is therefore recommended, simulating the same materials and structural configurations found in our heritage monuments, which forms the main area for future research work by the authors.

The present research has shown that Steel and Basalt Reinforced Mortar (SRM/BRM) and Polymer (SRP/BRP) are effective externally bonded composite solutions for masonry barrel vault retrofitting. The experimental campaign has shown that the four composite materials are effective solutions for the strengthening intervention, as they enable the masonry structure to carry substantial tensile stresses and prevent brittle failure. The structural responses, in terms of load and deformation capacity, were greatly increased (except for the final displacement of the BRM vault that was similar to the displacement of the non-strengthened vaults) and were similar to those obtained with the strengthening solutions based on an organic matrix (SRP/BRP). Moreover, the SRM/BRM water-vapour permeability, applicable over humid substrate, its lack of toxic substance emissions, fire resistance and ease of application and removability, unlike SRP/BRP, should also be highlighted. As a result, it has been demonstrated that SRM/BRM is a valid alternative solution for the retrofitting of masonry vaults, where the use of traditional strengthening systems are limited, even though its mechanical performance is not as efficient.

In addition, a spike anchorage system was introduced to prevent premature debonding of the externally bonded composites around the vault abutments, which is considered an important issue. No debonding of the strengthening materials (neither SRP/BRP nor SRM/BRM) was observed in the presence of normal stresses in that area, which underlines the effectiveness of the proposed solution. Nevertheless, the drilling of holes in many protected heritage buildings or structures may often be prohibited and alternative procedures represent a further area of research. Additional strengthening experiments involving numerical analyses are also planned, similar to the briefly described approach in this paper using Ring 3.0 software rather than conventional FE software.


## Acknowledgments

This research work was made possible thanks to financing from the EFFESUS Collaborative Project FP7 (G.A. Nº 314678) and the Basque Regional Government (IT781-13 research group). Furthermore, the authors wish to thank Javier Bengoechea, Josu Lucena, Stamatios Mihos, Vasileos Plamantouras and Antonio de Arcos for their kind contributions to this research work.


## References


[1] Valluzzi MR. *On the vulnerability of historical masonry structures: analysis and mitigation*. Materials and Structures 2007;40(7):723–43.

[2] Valluzzi MR, Modena C, de Felice G. *Current practice and open issues in strengthening historical buildings with composites.* Materials and Structures 2014;47:1971–85. DOI:10.1617/s11527-014-0359-7

[3] Ehsani MR. *Strengthening of earthquake-damaged masonry structures with composite materials.* In: Non-metallic (FRP) Reinforcement for Concrete Structures. Ed. L. Taerwe; 1995, 680-687.

[4] Schwegler G. *Masonry construction strengthened with fiber composites in seismically endangered zones.* In: Proceedings of 10th European Conference on Earthquake Engineering, Vienna, Austria 1994.

[5] Saadatmanesh H. *Fiber composites for new and existing structures*. ACI Structural Journal 1994;91(3):346-54. DOI: 10.14359/4363.

[6] Seible F. *Repair and seismic retest of a full-scale reinforced masonry building.* In: Proceedings of the 6th International Conference on Structural Faults and Repair 1995; Vol. 3, 229-236.

[7] Triantafillou TC. *Innovative strengthening of masonry monuments with composites*. In: Proceedings of 2nd International Conference Advanced Composite Materials in Bridges and Structures, Montreal, Quebec, Canada. 1996.

[8] Oliveira DV, Silva RA, Garbin E, Lourenço PB. *Strengthening of three-leaf stone masonry walls: an experimental research*. Materials and Structures 2012;45(8):1259–76. DOI: 10.1617/s11527-012-9832-3.

[9] Valluzzi MR and Modena C. *Experimental analysis and modelling of masonry vaults strengthened by FRP*. In: III Int. Seminar on Structural Analysis of Historical Constructions (SAHC-2001), Guimaraes (Portugal), 7-9 November 2001, 627-635.

[10] Foraboschi P. *Strengthening of Masonry Arches with Fiber-Reinforced Polymer Strips*. J. Compos. Constr. 2004;8(3):191–02. DOI:10.1061/(ASCE)1090-0268(2004)8:3(191).

[11] Lissel S. L. and Gayevoy A. *The use of FRP's in masonry: A state of the art review*. In Proceedings. In: International Conference on the Performance of Construction Materials, Cairo, Egypt; 2003, pp. 1243–1252.

[12] Oliveira D, Basilio I, Lourenço P. *FRP strengthening of masonry arches towards an enhanced behaviour*. Bridge maintenance, safety, Management, Life Cycle Performance and Cost – Cruz, Frangopol & Neves (eds); 2006. Taylor & Francis Group, London, ISBN 0415403154.

[13] Larrinaga P, Chastre C, Biscaia HC, San-José JT. *Experimental and numerical modelling of basalt textile reinforced mortar behavior under uniaxial tensile stress.* Materials and Design 2014;55:66–74. DOI:10.1016/j.matdes.2013.09.050.

[14] Olivito RS, Cevallos OA, Carrozzini A. *Development of durable cementitious composites using sisal and flax fabrics for reinforcement of masonry structures*. Materials and Design 2014;57:258–68. DOI:10.1016/j.matdes.2013.11.023.

[15] De Santis S, De Felice G. *Tensile behaviour of mortar-based composites for externally bonded reinforcement systems.* Composites Part B: Engineering 2015;68:401-13. DOI:10.1016/j.compositesb.2014.09.011.

[16] Garmendia L, Larrinaga P, García D, Marcos I. *Textile-Reinforced Mortar as Strengthening Material for Masonry Arches*. International Journal of Architectural Heritage: Conservation, Analysis, and Restoration 2014;8(5):627-48. DOI: 10.1080/15583058.2012.704480

[17] Garmendia L, Marcos I, Garbin E, Valluzzi MR. *Strengthening of masonry arches with Textile-Reinforced Mortar: experimental behaviour and analytical approaches*. Materials and Structures 2014;47(12):2067–80. DOI:10.1617/s11527-014-0339-y.

[18] Bernat E, Gil L, Roca P, Escrig C. *Experimental and analytical study of TRM strengthened brickwork walls under eccentric compressive loading*. Constr Build Mater 2013;44:35–47. DOI:10.1016/j.conbuildmat.2013.03.006.

[19] Triantafillou T. and Papanicolau C. *Textile Reinforced Mortars (TRM) versus Fiber Reinforced Polymers (FRP) as strengthening materials of concrete structures*. In: FRPRCS-7, ACI SP-230, 2005, Kansas City, USA, 99-118.

[20] Borri A, Castori G, Grazini A. *Seismic upgrading of historical masonry buildings with steel reinforced grout (SRG).* In: *Proceedings of FRPRCS-8.* Patras, Greece, July 16-18, 2007. University of Patras, Patras, Greece.

[21] Borri A, Casadei P, Castori G, Hammond J. *Strengthening of brick masonry arches with externally bonded steel reinforced composites*. Journal of Composites for Construction 2009;13(6):468-75. DOI:10.1061/(ASCE)CC.1943-5614.0000030.

[22] EN 772-1:2001. Methods of test for masonry units - Part 1: Determination of compressive strength.

[23] UNI6556:1976. Tests of concretes. Determination of static modulus of elasticity in compression.

[24] EN 67042:1988 Big ceramics pieces of burned clay. Determination of the modulus of rupture.

[25] UNE-EN 1015-11:2000. Methods of test for mortar for masonry - Part 11: Determination of flexural and compressive strength of hardened mortar.

[26] ASTM C 469:2002. Standard test method for static modulus of elasticity and Poisson's ratio of concrete in compression.

[27] Larrinaga P, Chastre C, San-José JT, Garmendia L. Non-linear analytical model of composites based on basalt textile reinforced mortar under uniaxial tension, Composites: Part B 2013;55:518–27. DOI:10.1016/j.compositesb.2013.06.043.

[28] Banibayat P, Patnaik A. *Variability of mechanical properties of basalt fiber reinforced polymer bars manufactured by wet-layup method*. Materials and Design 2014;56:898–06. DOI:10.1016/j.matdes.2013.11.081.

[29] Fiore V, Scalici T, Di Bella G, Valenza A. *A review on basalt fibre and its composites*. Composites Part B 2015;74:74-94.

[30] ASTM D 5034-95(2001). Standard test method for breaking strength and elongation of textile fabrics (Grab Test).

[31] Cevallos OA, Olivito RS. *Effects of fabric parameters on the tensile behaviour of sustainable cementitious composites.* Composites Part B: Engineering 2014;69:256-66. DOI:10.1016/j.compositesb.2014.10.004.

[32] García D. *Experimental and numerical analysis of stone masonry walls strengthened with advanced composite materials*. PhD Thesis. Escuela de Ingeniería de Bilbao, 2009.

[33] Haüßler-Combe U, Hartig J. *Bond and failure mechanism of Textile Reinforced Concrete (TRC) under uniaxial tensile loading*. Cement and Concrete Composites 2007;29:279–89. DOI:10.1016/j.cemconcomp.2006.12.012

[34] Contamine R, Si Larbi A, Hamelin P. *Contribution to direct tensile testing of textile reinforced concrete (TRC) composites*. Materials Science Engineering A 2011;528:8589–98. DOI:10.1016/j.msea.2011.08.009

[35] Larrinaga P. Flexural strengthening of low grade concrete through the use of new cement-based composite materials. PhD thesis, University of the Basque Country, Spain; 2011.

[36] Heyman J. *The masonry arch.* Ellis Horwood Limited, 1982.

[37] Bednarz Ł, Górski A, Jasieńko J, Rusiński E. *Simulations and analyses of arched brick structures.* Automation in Construction 2011;20:741-54. DOI:10.1016/j.autcon.2011.01.005.

[38] Bednarz ŁJ, Jasieńko J, Rutkowski M, Nowak TP. *Strengthening and long-term monitoring of the structure of an historical church presbytery*. Engineering Structures 2014;81:62–75. DOI:10.1016/j.engstruct.2014.09.028.

[39] Briccoli Bati S, Rovero L. *Towards a methodology for estimating strength and collapse mechanism in masonry arches strengthened with fibre reinforced polymer applied on external surfaces.* Materials and Structures 2008;41(7):1291–06. DOI:10.1617/s11527-007-9328-8.

[40] Bernat-Maso E, Gil L, Marcé-Nogué J. *The structural performance of arches made of few vossoirs with dry-joints*. Structural Engineering and Mechanics 2012;44(6):775-99.

[41] D'Ambrisi A, Feo L, Focacci F. *Experimental and analytical investigation on bond between Carbon-FRCM materials and masonry*. Composites Part B: Engineering 2013;46:15–20. DOI:10.1016/j.compositesb.2012.10.018.

[42] Valluzzi MR, Oliveira DV, Caratelli A et al. *Round Robin Test for composite-to-brick shear bond characterization.* Materials and Structures 2012;45:1761-91. DOI: 10.1617/s11527-012-9883-5.

[43] De Felice G, De Santis S, Garmendia L, Ghiassi B, Larrinaga P, Lourenc PB¸ Oliveira DV, Paolacci F, Papanicolaou CG. *Mortar-based systems for externally bonded strengthening of masonry*. Materials and Structures 2014;47:2021–37. DOI:10.1617/s11527-014-0360-1.

[44] Garmendia L. 2010. Rehabilitation of masonry arches by a compatible and minimally invasive strengthening system. PhD thesis, University of the Basque Country, Spain; 2010.

[45] Triantafillou T.C. (1998). Strengthening of masonry structures using epoxy-bonded FRP laminates. ASCEJ. Compos. for Constr. 1998;2(2):96-104.

[46] Triantafillou T.C. (1998b). Errata in article: Strengthening of masonry structures using epoxy-bonded FRP laminates. ASCEJ Compos. for Constr. 1998b;2(2):96-104.

[47] Roca P, López-Almansa F, Miquel J, Hanganu A. Limit analysis of reinforced masonry vaults. Engineering Structures 2007;29:431–9.

[48] Garcia D, San-Jose JT, Garmendia L, San-Mateos R. *Experimental study of traditional stone masonry under compressive load and comparison of results with design codes*. Materials and Structures 2012;45:995–1006. DOI:10.1617/s11527-011-9812-z.

**Figure 1**

**Click here to download high resolution image**

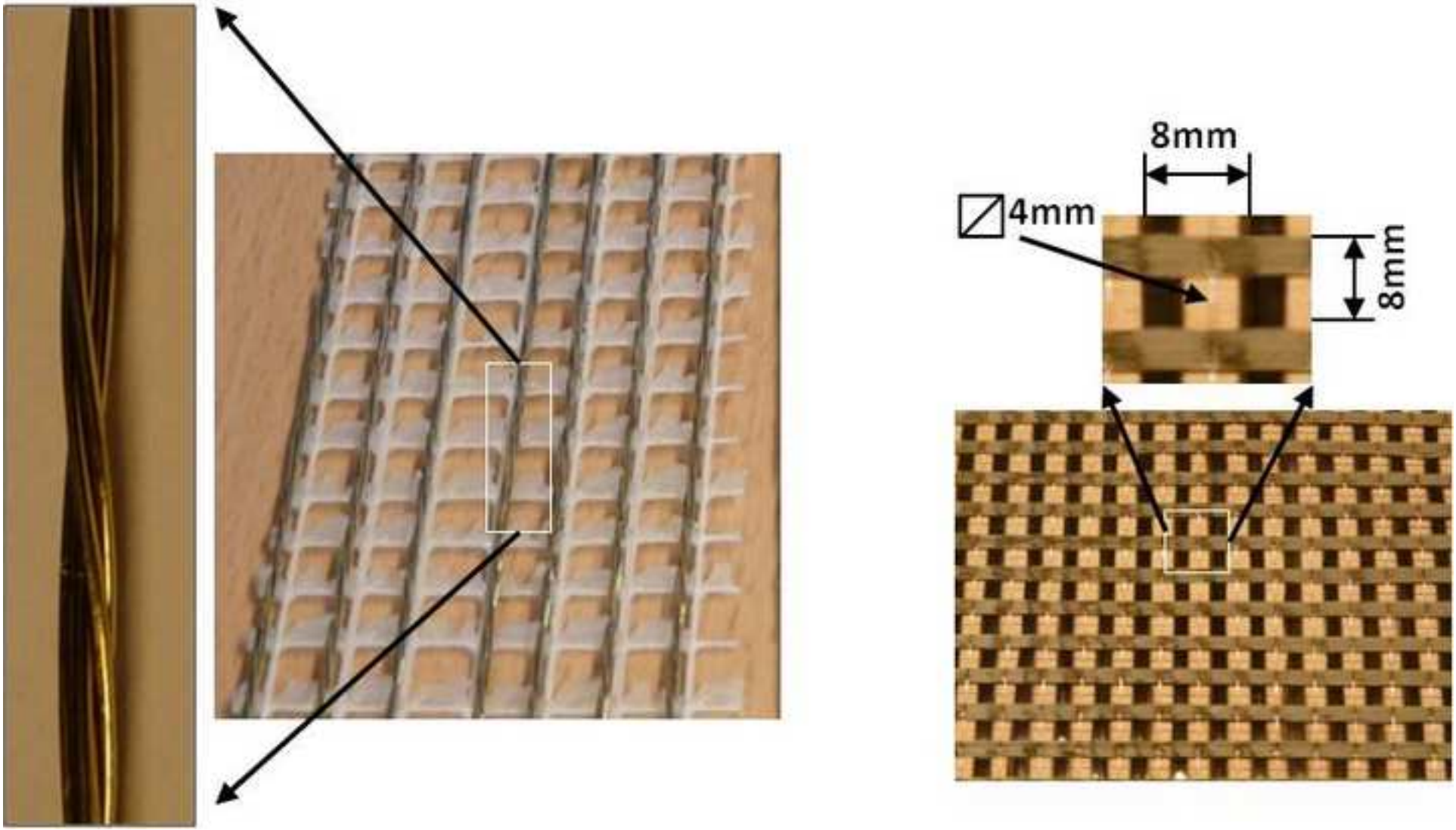

Figure 2

Click here to download high resolution image

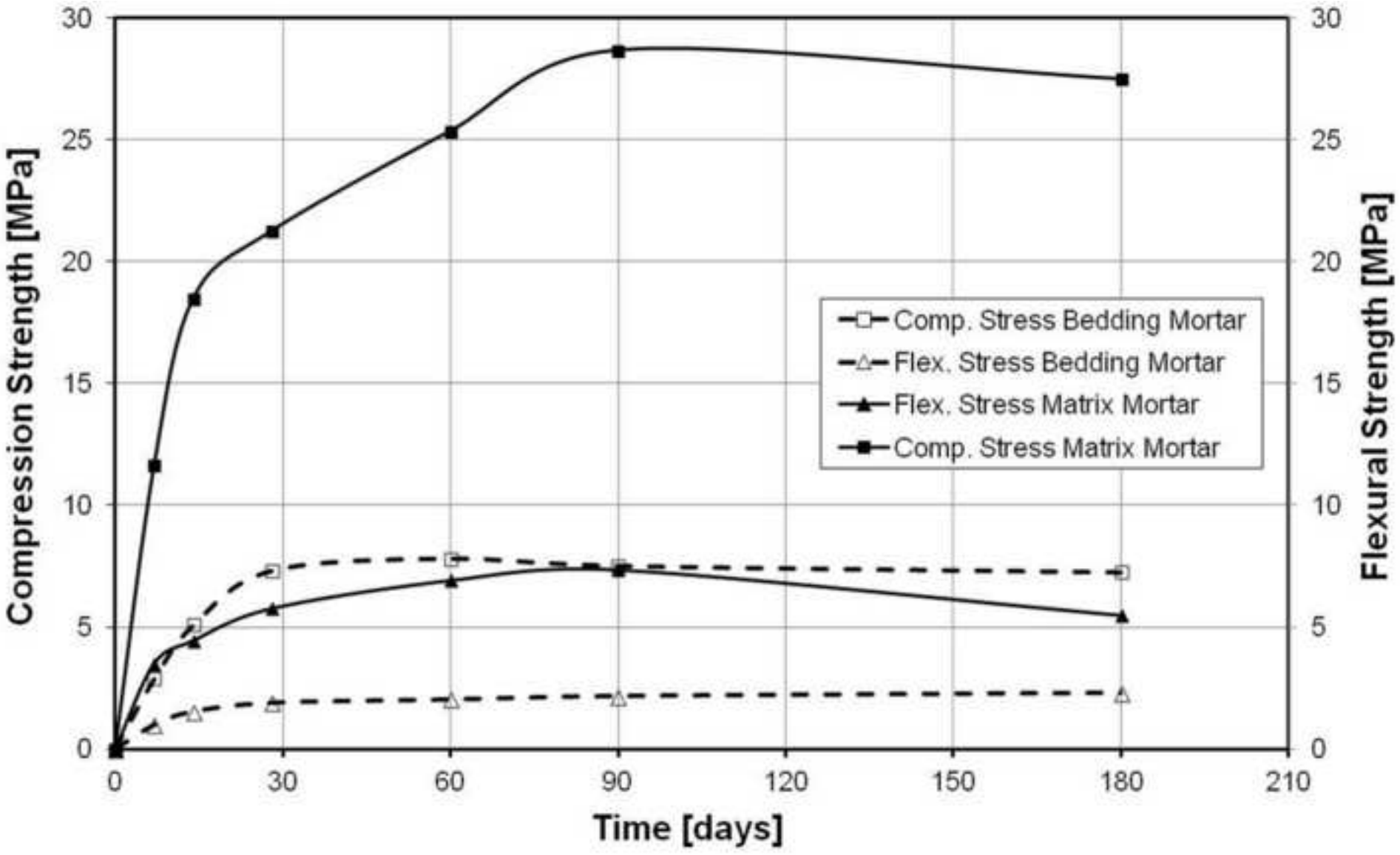

**Figure 3**

**Click here to download high resolution image**

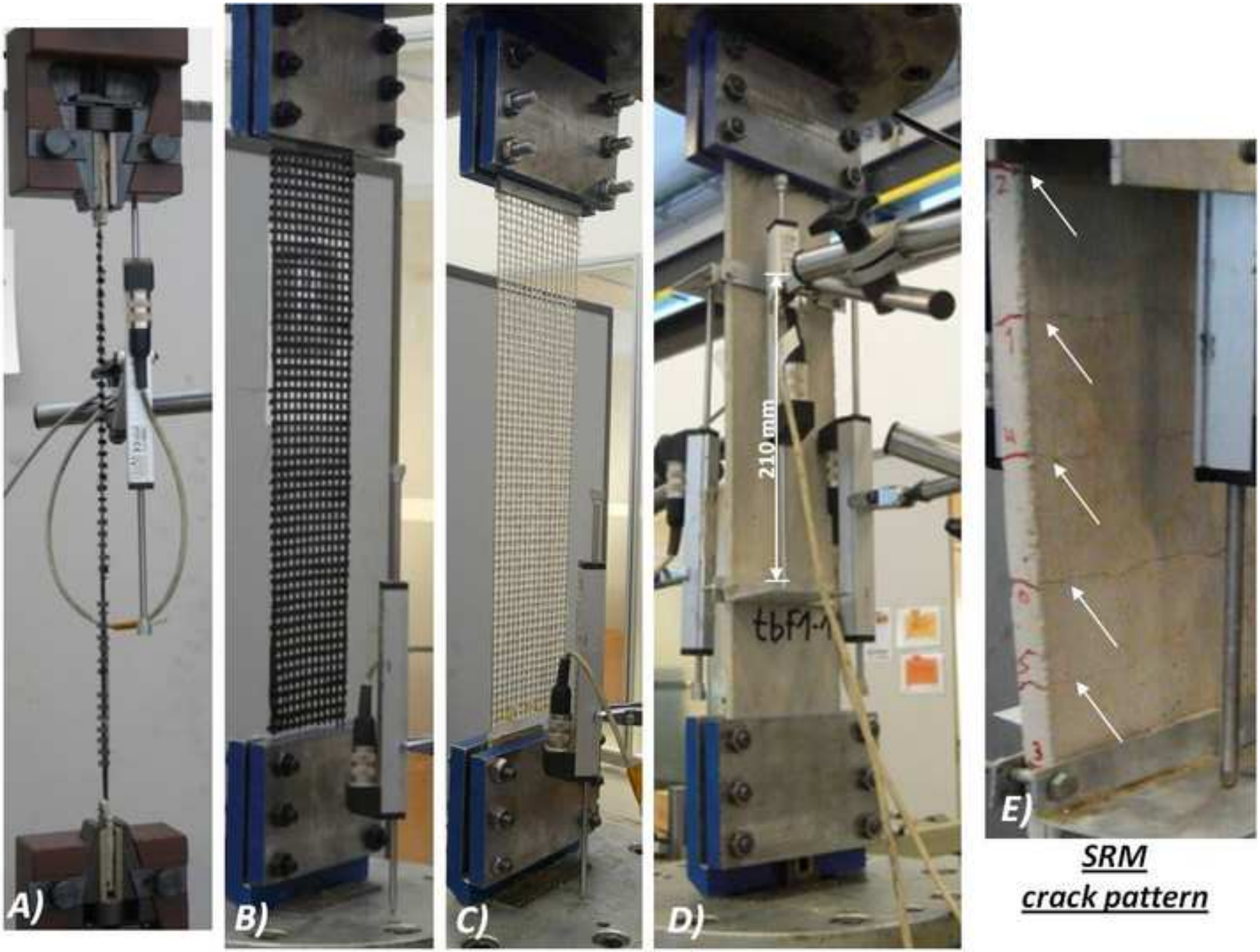

**Figure 4**

Click here to download high resolution image

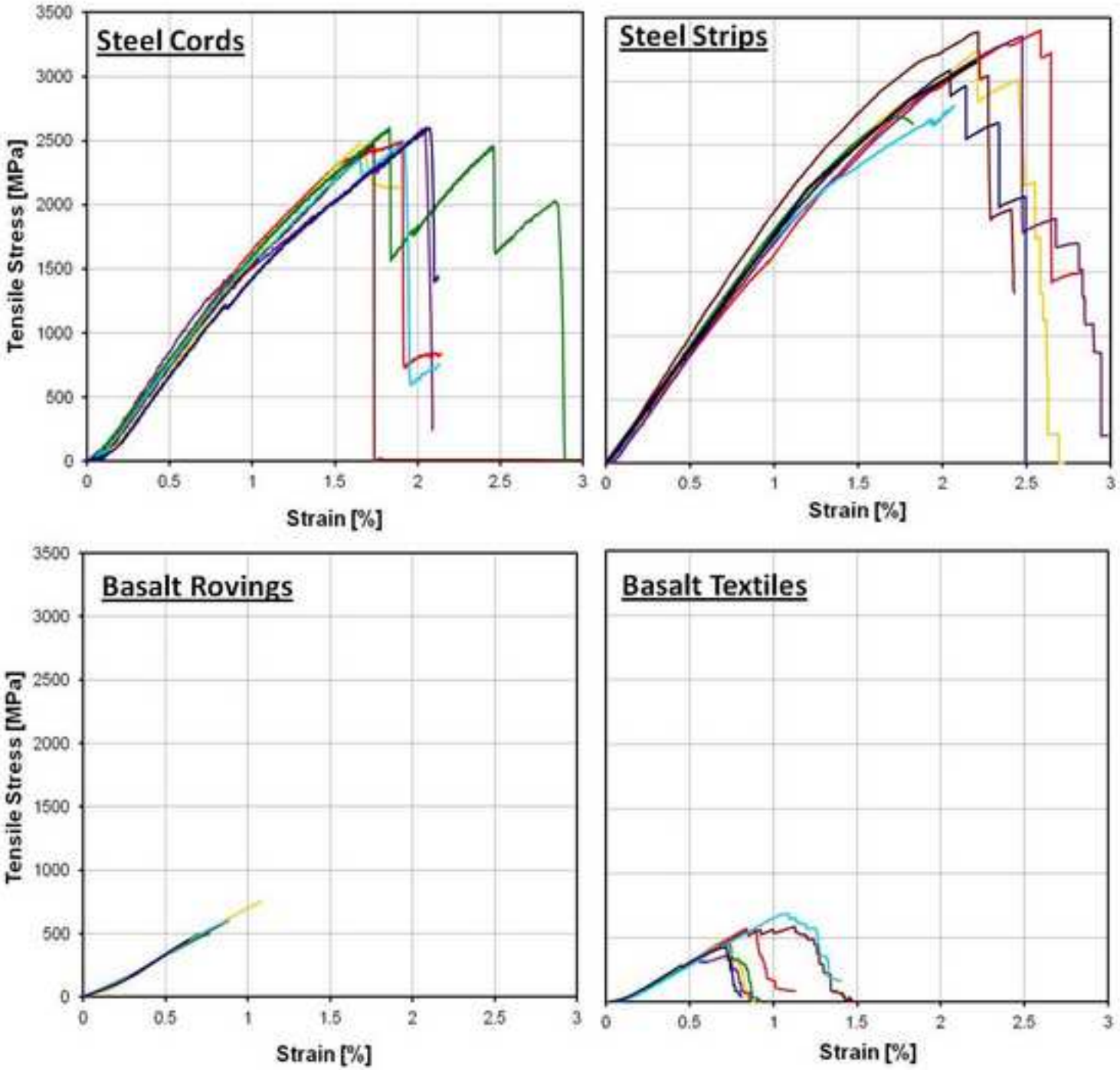

**Figure 5**

**Click here to download high resolution image**

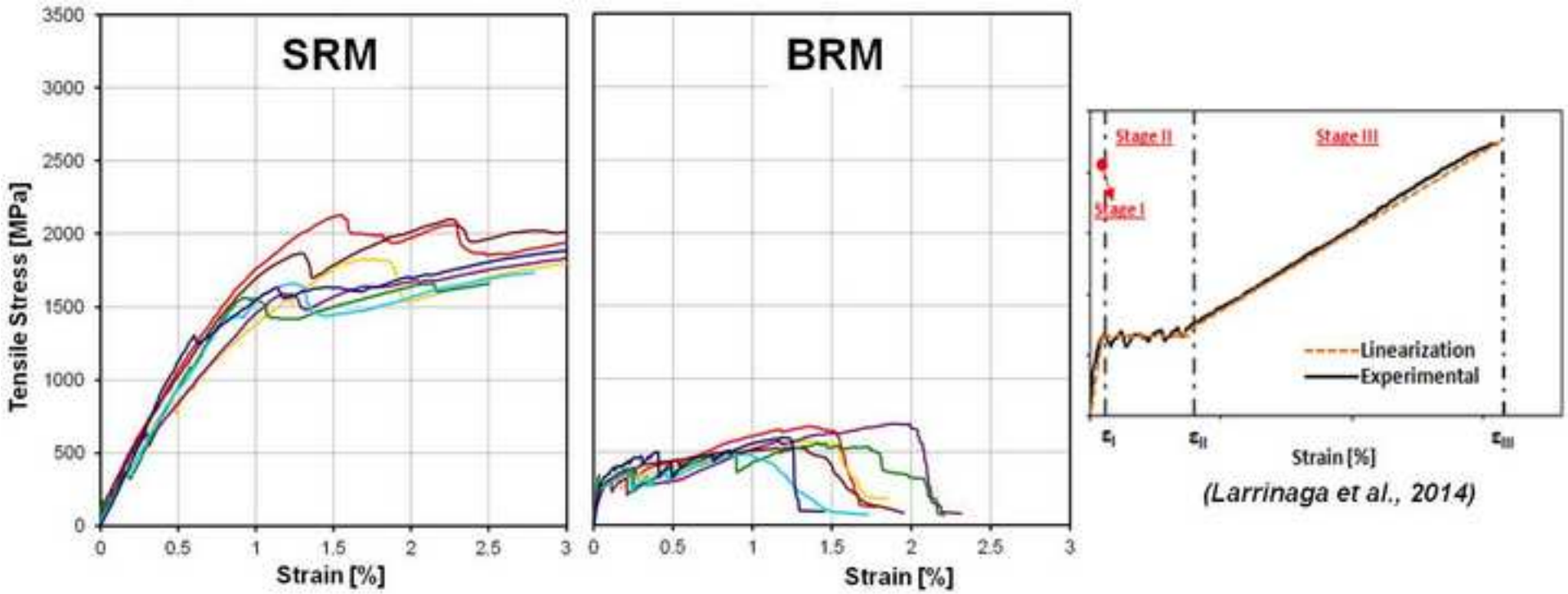

**Figure 6**

Click here to download high resolution image

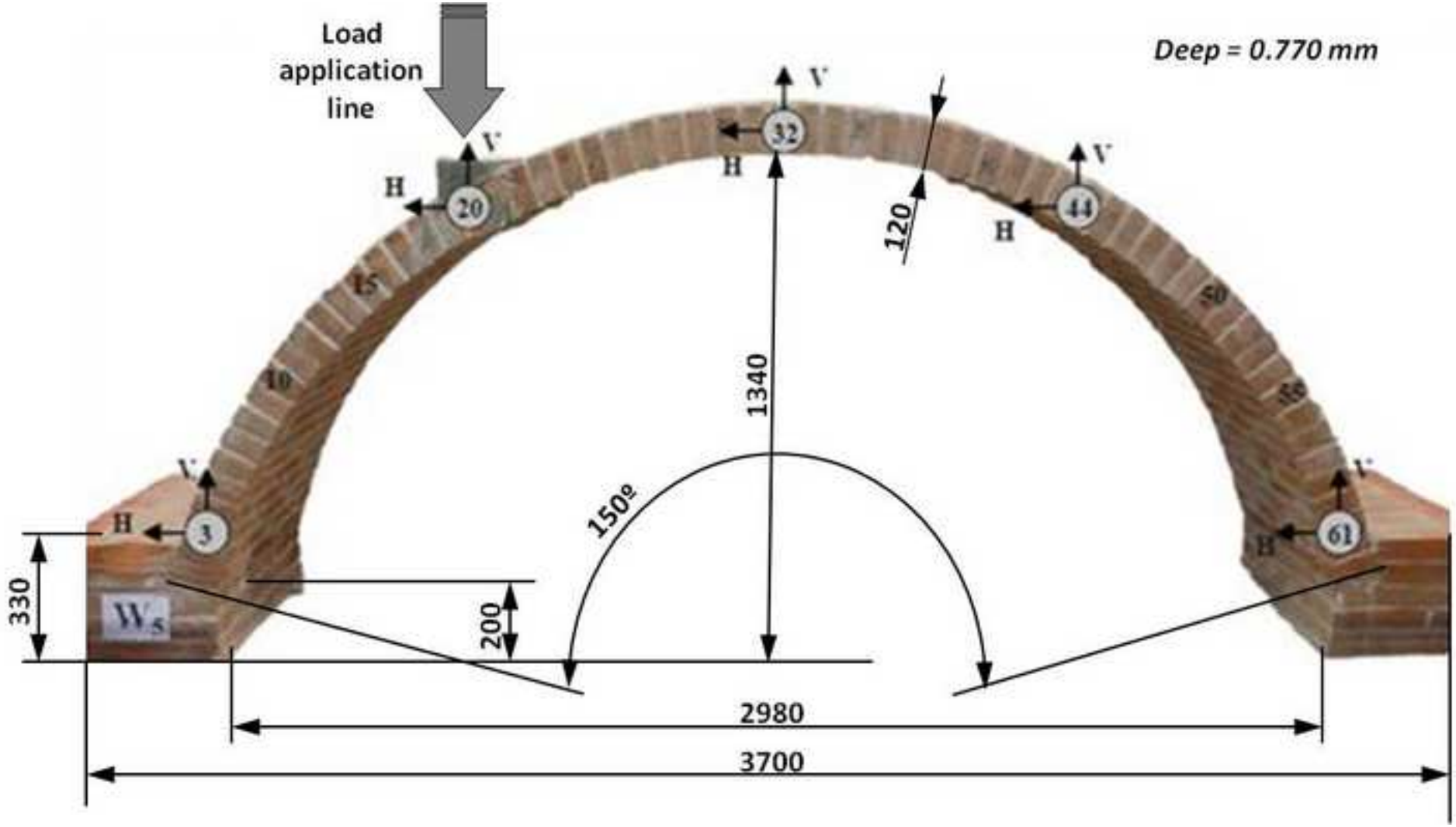

**Figure 7**

**Click here to download high resolution image**

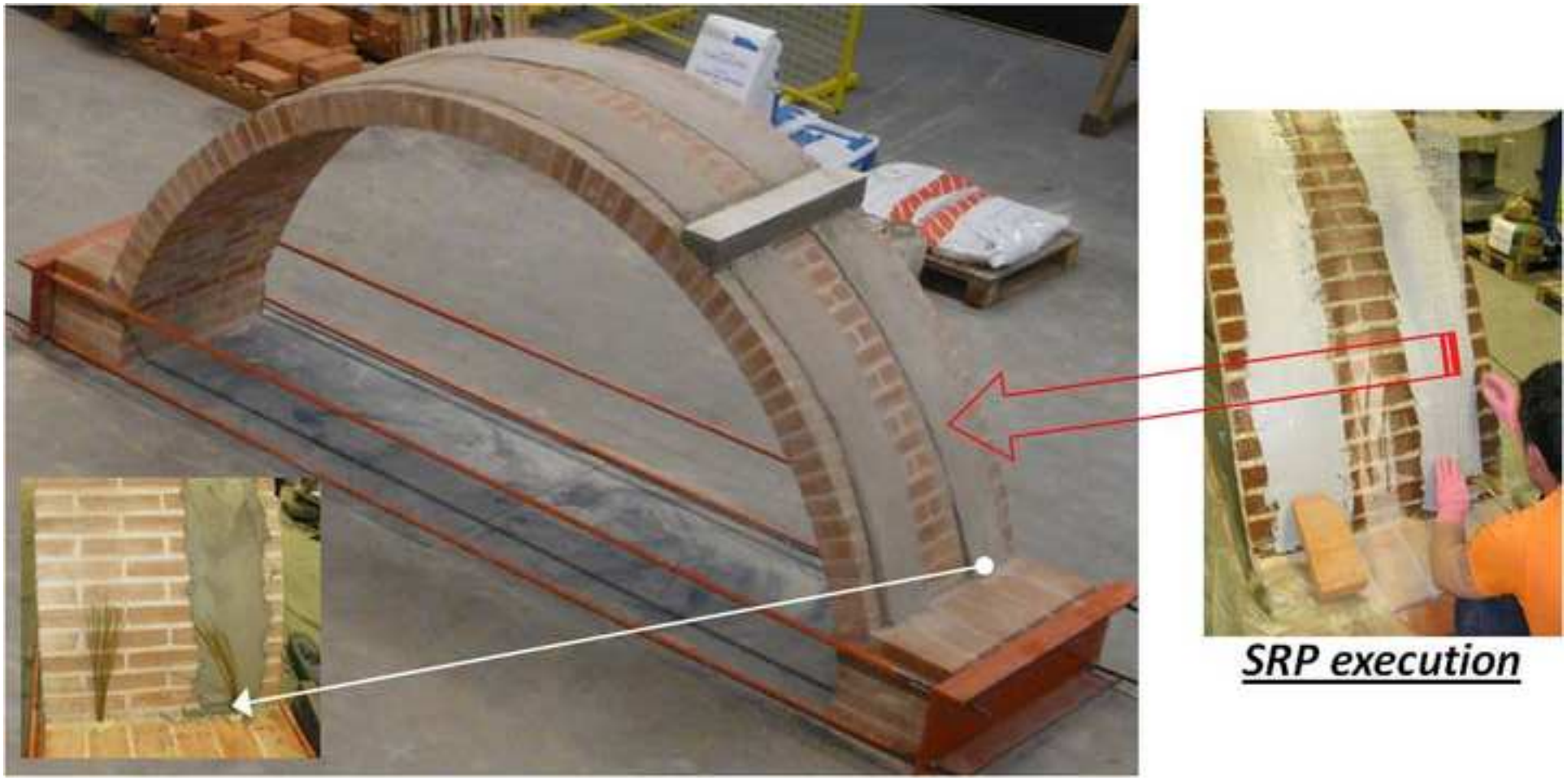

**Figure 8**

**Click here to download high resolution image**

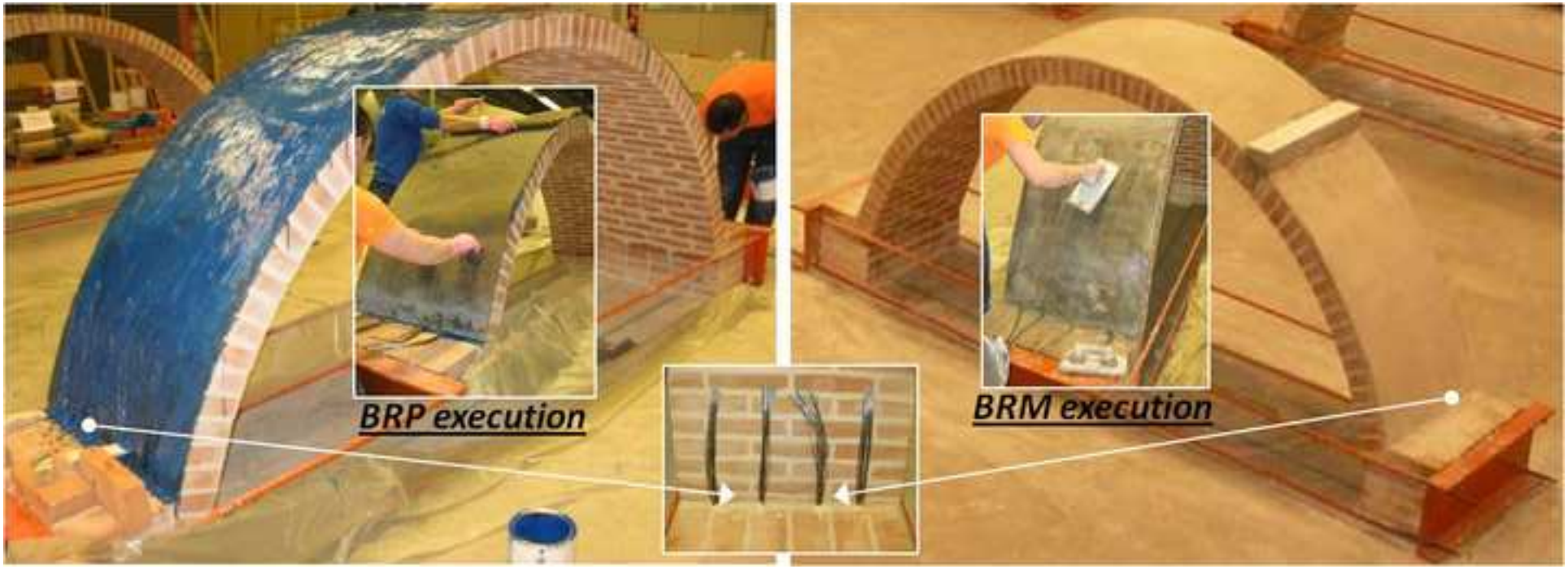

**Figure 9**

**Click here to download high resolution image**

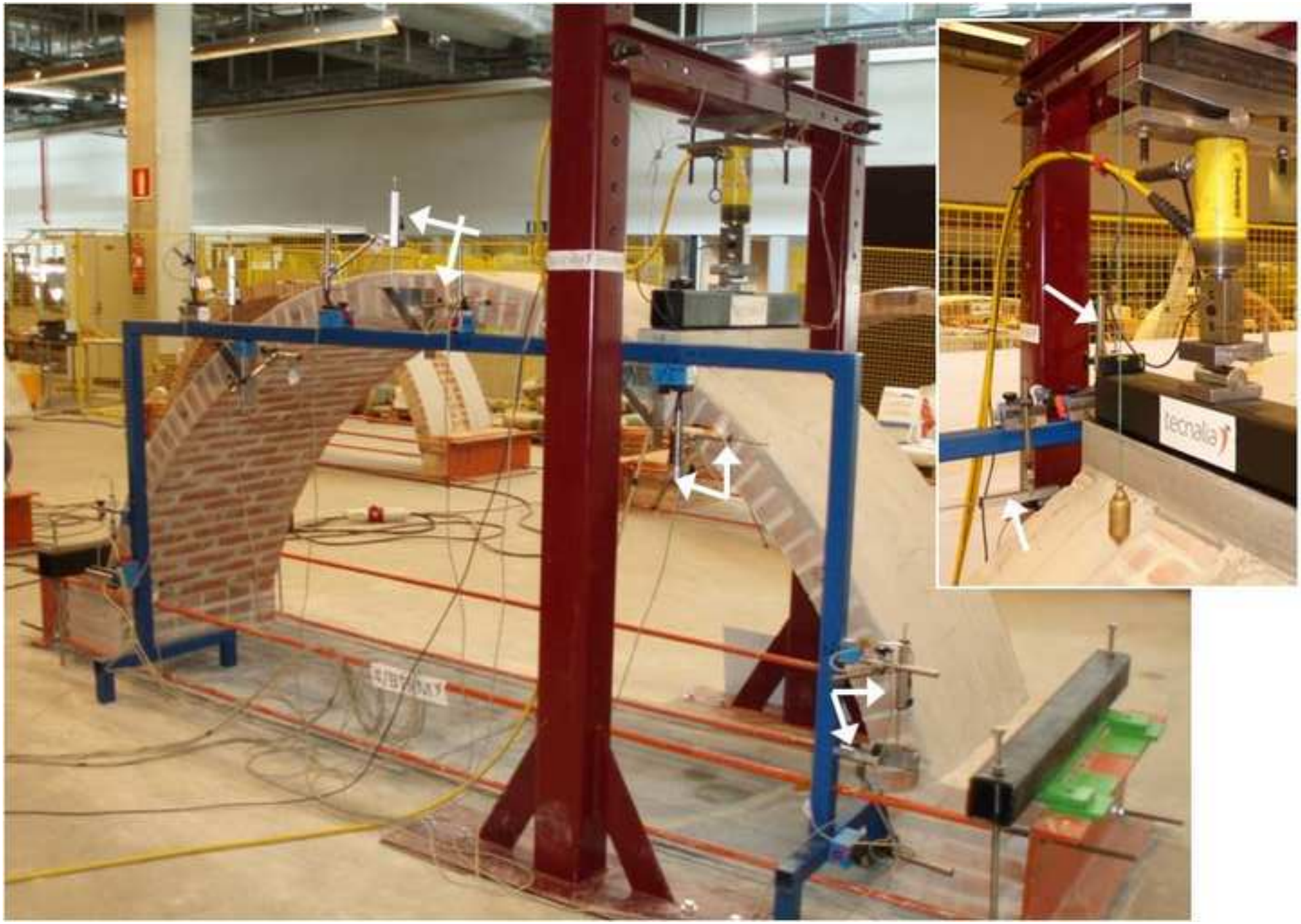

**Figure 10**

**Click here to download high resolution image**

Figure 11

Click here to download high resolution image

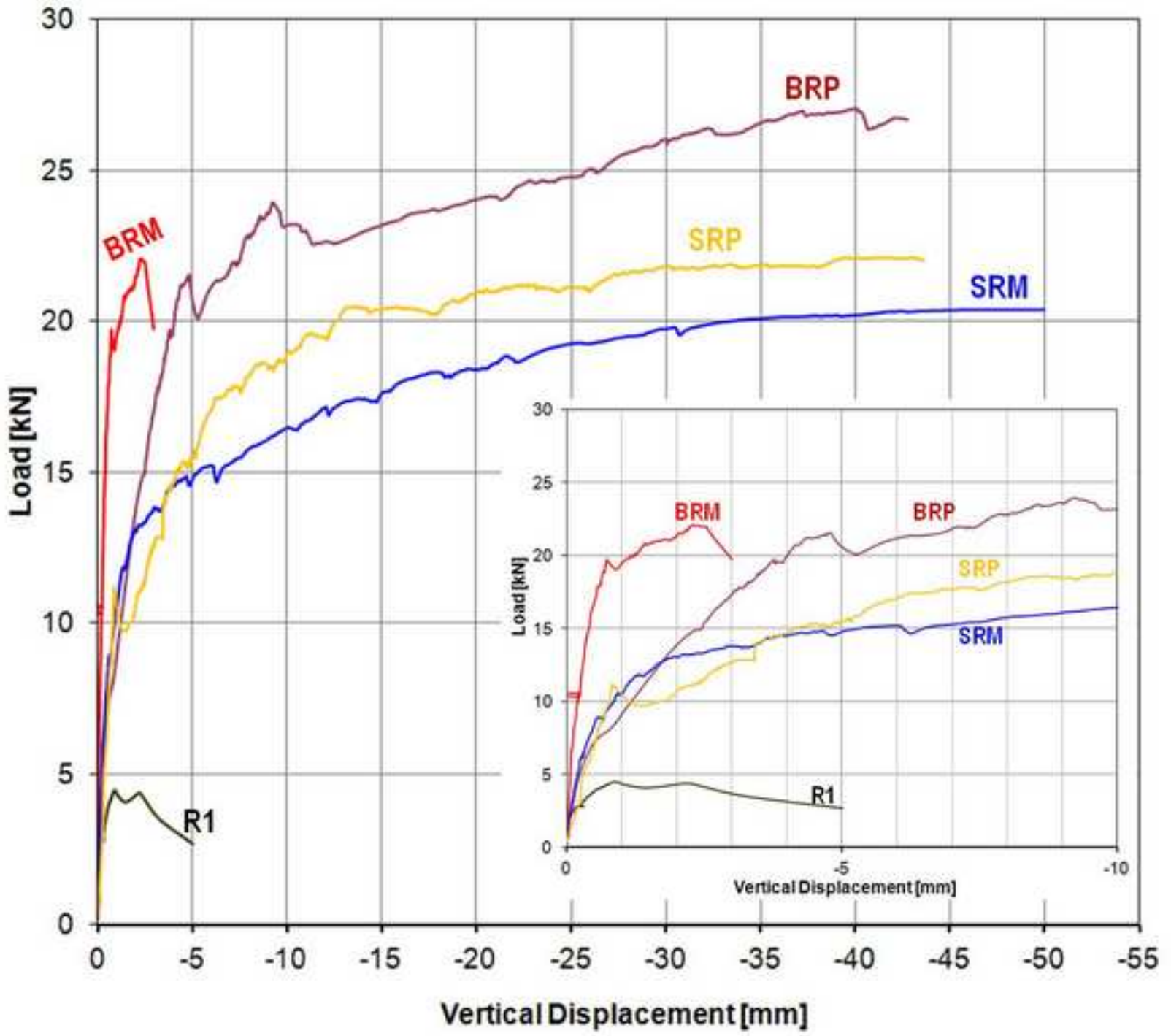

**Figure 12**

**Click here to download high resolution image**